

RESEARCH

Open Access



Potential predictive value of CD8A and PGF protein expression in gastric cancer patients treated with neoadjuvant immunotherapy

Chengjuan Zhang^{1,3†}, Tingjie Wang^{2†}, Jing Yuan^{1†}, Tao Wang⁴, Bin Ma⁵, Benling Xu⁶, Ruihua Bai⁷, Xiance Tang⁸, Xiaojie Zhang⁶, Minqing Wu¹, Tianqi Lei¹, Wenhao Xu¹, Yongjun Guo^{2,3*} and Ning Li^{9*}

Abstract

Background Immunoneoadjuvant therapy has gained significant attention due to its remarkable advancements in cancer treatment. This study aimed to investigate the molecular mechanisms underlying immunoneoadjuvant therapy through a comprehensive multiomics analysis of samples from a registered clinical trial cohort.

Methods Preoperative samples were collected from 16 patients, and postoperative samples were obtained from 12 among them. RNA sequencing (RNA-seq) and Olink proteomics were employed to identify key genes before and after neoadjuvant treatment. The weighted coexpression network was constructed using Weighted gene co-expression network analysis (WGCNA). Furthermore, the proportion of infiltrated immune cells was calculated using xCell based on normalized expression data derived from RNA-seq.

Results Patients were stratified into T1 (good efficacy) and T2 (poor efficacy) groups based on Tumor Regression Grade (TRG) to neoadjuvant immunotherapy. Compared to the T2 group (TRG2 and TRG3), the T1 group (TRG0 and TRG1) showed significant differences in pathways related to inflammatory response and myeloid leukocyte activation. Furthermore, the T1 group exhibited elevated levels of CD8⁺ T cells and B cells. The top two factors with the highest area under the Receiver Operating Characteristic (ROC) curve were CD8a molecule (CD8A) (1.000) and C-C motif chemokine ligand 20 (CCL20) (0.967). Additionally, the expression of placenta growth factor (PGF) and TNF receptor superfamily member 21 (TNFRSF21) proteins significantly increased in the T1 group compared to the T2 group. High expression of CD8A and PGF were associated with favorable and poor prognosis in gastric cancer patients, respectively. Immunoinfiltration analysis revealed a positive correlation between CD8A and dendritic cell (DC) levels, while a negative correlation was observed with myeloid-derived suppressor cell (MDSC) levels.

[†]Chengjuan Zhang, Tingjie Wang and Jing Yuan contributed equally to this work.

*Correspondence:
Yongjun Guo
yongjunguo@hotmail.com
Ning Li
lining97@126.com

Full list of author information is available at the end of the article



© The Author(s) 2025. **Open Access** This article is licensed under a Creative Commons Attribution-NonCommercial-NoDerivatives 4.0 International License, which permits any non-commercial use, sharing, distribution and reproduction in any medium or format, as long as you give appropriate credit to the original author(s) and the source, provide a link to the Creative Commons licence, and indicate if you modified the licensed material. You do not have permission under this licence to share adapted material derived from this article or parts of it. The images or other third party material in this article are included in the article's Creative Commons licence, unless indicated otherwise in a credit line to the material. If material is not included in the article's Creative Commons licence and your intended use is not permitted by statutory regulation or exceeds the permitted use, you will need to obtain permission directly from the copyright holder. To view a copy of this licence, visit <http://creativecommons.org/licenses/by-nc-nd/4.0/>.

Conclusions Through multiomics analysis, we discovered that CD8A is linked to enhanced treatment response and tumor regression. In contrast, PGF appears to exert adverse effects on treatment outcomes, suggesting a complex interplay of factors influencing the efficacy of immunoneoadjuvant therapy in gastric cancer.

Keywords Gastric adenocarcinoma, Neoadjuvant immunotherapy, Sintilimab, Olink proteomics, CD8A, PGF

Introduction

Gastric cancer remains a significant global health concern, ranking fifth in incidence and fourth in mortality worldwide [1]. Despite advancements in tumor therapy, the subtle and atypical clinical symptoms of early gastric cancer contribute to over 60% of patients developing local or distant metastasis at the time of diagnosis [2]. Currently, radical surgical resection can effectively cure the disease in patients with early-stage gastric cancer. However, for those with locally advanced gastric cancer, even with interventions such as radiotherapy and chemotherapy, the 5-year survival rate sharply decreases [3–5]. Therefore, the need for new treatments becomes particularly imperative.

The combination of immunotherapy and chemotherapy has established itself as the standard first-line treatment for advanced gastric cancer. In the CheckMate-649 trial evaluating Nivolumab, patients treated with combination chemotherapy exhibited significantly longer median overall survival (OS) and median progression-free survival (PFS) compared to those treated with chemotherapy alone [6]. Given the notable efficacy of immunotherapy in advanced gastric cancer, numerous clinical studies have explored whether incorporating immunotherapy into perioperative treatment can enhance the survival time of patients with locally advanced gastric cancer. A Phase III study, Keynote585, presented at the ESMO meeting in 2023, indicated that increased perioperative immunotherapy improved event-free survival (EFS) and pathological complete response (pCR) rates in patients but did not demonstrate a survival advantage over placebo. Identifying individuals who truly benefit from immunotherapy is a pivotal consideration in its current application during the perioperative period. To address this, we conducted a Phase II clinical study evaluating the perioperative treatment of locally advanced gastric cancer using sintilimab in combination with Fluorouracil, Leucovorin, Oxaliplatin, and Docetaxel (FLOT) (Clinical trial number: NCT04341857). Sintilimab (also known by its trade name Tyvyt) is a fully human monoclonal antibody that targets the programmed cell death protein 1 (PD-1) receptor. Preliminary results indicate that sintilimab combined with FLOT neoadjuvant therapy achieved an 17.2% pCR rate of tumor regression grade (TRG) group [7]. The study also observed variable responses among patients, with some achieving pCR and others not. Currently, much debate is ongoing regarding which indicators serve as reliable predictors of immunotherapy efficacy.

Subgroup analysis revealed that patients with higher Combined Positive Score (CPS) scores of programmed cell death-ligand 1 (PD-L1) exhibited a more favorable therapeutic effect, and PD-L1 expression levels were significantly higher on CD8⁺ T cells than on CD4⁺ T cells. However, the expression of PD-L1 is not exactly consistent with the efficacy of immunotherapy [8–10]. Blood specimens, offering the advantages of convenience and multiple sampling compared to tissue specimens, have been explored for potential predictive indicators of immunotherapy efficacy. Other studies indicated that cytokines in the blood might also serve as predictors of immunotherapy effectiveness. In our clinical studies, we collect blood samples from patients to identify indicators of treatment efficacy. Protein biomarkers are the cornerstones in disease prediction, diagnosis, and prevention. The advent of high-throughput proteomics enables the simultaneous quantification of numerous proteins. However, the vast amount of data acquired poses challenges for analysis, and the potential for false positive results complicates subsequent validation efforts. Recently, Olink technology has gained popularity for providing multiple detection panels targeting various disease processes. Its requirement for small sample volumes is particularly advantageous when clinical samples are limited. Furthermore, it can capture a broad spectrum of proteins across the entire dynamic range (>10 logs). A previous study demonstrated that Olink proteomics exhibits excellent repeatability and stability in detecting proteins in plasma samples [11, 12]. In the current study, Olink proteomics was employed to identify inflammation-associated proteins that showed differences before and after neoadjuvant therapy, aiming to identify potential markers for treatment response.

This study employed a comprehensive omics analysis to discern key molecular characteristics associated with the efficacy of sintilimab combined with FLOT neoadjuvant therapy for gastric/gastroesophageal junction adenocarcinoma. This involved analyzing differential proteins before and after neoadjuvant therapy and among different therapeutic groups. The study further investigated the interplay between relevant molecules and immune cell infiltration, laying the groundwork for the clinical treatment and efficacy evaluation of gastric/gastroesophageal junction adenocarcinoma.

Materials and methods

Patient and sample collection

Plasma samples were collected from 16 enrolled patients who visited The Affiliated Cancer Hospital of Zhengzhou University (Henan Cancer Hospital) between August 10, 2019, and July 15, 2020, before and after treatment, following a standardized treatment regimen. The study received approval from the ethics committee of The Affiliated Cancer Hospital of Zhengzhou University and was conducted in accordance with local ethical guidelines, and informed consent for participation in the study has been obtained from all participants.

Each patient underwent four cycles of the FLOT regimen, which included docetaxel 50 (mg/m²), oxaliplatin 80 (mg/m²), leucovorin 200 (mg/m²), and fluorouracil 2600 (mg/m²) administered as a continuous 24-hour intravenous infusion on day 1, with one cycle every two weeks. This was combined with three cycles of sintilimab (200 mg, intravenous infusion, day 1, one cycle every 3 weeks). Following neoadjuvant therapy, radical resection was performed, and patients received four additional cycles of adjuvant therapy using the FLOT regimen. The characteristics of the 16 patients are detailed in Table 1.

Peripheral anticoagulant blood (2 mL, 1600 g) was collected from each patient before the first and second neoadjuvant therapy. Centrifugation was performed for 15 min to obtain upper plasma and middle white membrane. The upper plasma was carefully drawn and dispensed into 2 mL frozen storage tubes (1 mL/tube) and stored at -80 °C for future use. The Buffy Coat in the middle layer was meticulously absorbed and frozen at -80 °C. All the aforementioned procedures were completed within 2 h of blood collection.

RNA-seq analysis

Total RNA was isolated using Trizol (Invitrogen), followed by purification with QIAGEN RNeasy and treatment with RNase-free DNAase (QIAGEN). The process encompassed library preparation and sequencing experiments, and the sequencing results were imported into ACGT101-miR (LC Sciences, Houston, Texas, USA) for analysis. The mRNA and small RNA-seq libraries were prepared and used. The analysis process began with the removal of 3' adapters and unwanted sequences to obtain clean data. Length screening was performed, retaining sequences with base lengths between 18 and 26 nucleotides. The obtained sequences underwent comparison with various RNA databases (mRNA, RFam, and Rепbase databases, excluding miRNA) and were filtered to obtain valid data. Subsequently, miRNA identification and differentiation analysis were conducted by comparing precursors and the genome, leading to the final prediction of target genes for the different miRNAs. The TruSeq Small RNA Sample Preparation Kits (Illumina, San Diego,

Table 1 The clinicopathological features of 16 patients

No.	Age/Sex	Olink		RNA-seq		TRG	ypTNM	Histological type	Tumor site	Differentiated degree	pCR	PDL1
		BF	AF	BF	AF							
1	45/Male	Yes	Yes	Yes	Yes	TRG2	ypT3N3aM0	Adenocarcinoma	Body	poorly differentiated	Yes	5
2	66/Female	Yes	Yes	No	No	TRG1	ypT4aN0M0	Adenocarcinoma	Antrum	poorly differentiated	No	1
3	55/Male	Yes	Yes	Yes	Yes	TRG1	ypT1N1M0	Adenocarcinoma	Cardia	moderately differentiated	Yes	/
4	42/Male	Yes	Yes	No	No	TRG3	ypT3N1M0	Adenocarcinoma	Body	Medium-low differentiated	No	30
5	57/Female	Yes	Yes	No	No	TRG2	ypT2N1M0	Adenocarcinoma	Antrum	moderately differentiated	No	<1
6	49/Male	Yes	Yes	Yes	Yes	TRG1	ypT1N0M0	Adenocarcinoma	Cardia	poorly differentiated	Yes	10
7	58/Male	Yes	Yes	Yes	Yes	TRG2	ypT1N2M0	Adenocarcinoma	Cardia	moderately differentiated	Yes	5
8	61/Male	Yes	Yes	No	No	TRG2	ypT3N1M0	Adenocarcinoma	Whole stomach	poorly differentiated	No	5
9	66/Male	Yes	Yes	Yes	Yes	TRG3	ypT3N2M0	Adenocarcinoma	Cardia	poorly differentiated	Yes	<1
10	69/Male	Yes	Yes	Yes	Yes	TRG0	ypT0N0M0	Adenocarcinoma	Cardia	moderately differentiated	Yes	<1
11	57/Male	Yes	Yes	No	No	TRG3	ypT3N1M0	Adenocarcinoma	Cardia	moderately differentiated	No	1
12	50/Female	Yes	Yes	Yes	Yes	TRG1	ypT1N1M0	Adenocarcinoma	Cardia	moderately differentiated	Yes	5
13	66/Male	Yes	No	Yes	Yes	TRG2	ypT3N2M0	Adenocarcinoma	Cardia	poorly differentiated	Yes	<1
14	58/Male	Yes	No	No	No	TRG0	ypT0N0M0	Adenocarcinoma	Antrum	poorly differentiated	No	/
15	55/Male	Yes	No	No	No	TRG2	ypT3N0M0	Adenocarcinoma	Cardia	Low-medium differentiation	No	<1
16	45/Male	Yes	No	Yes	Yes	TRG2	ypT2N0M0	Adenocarcinoma	Cardia	poorly differentiated	Yes	30

/: No residual tumor cells were found

USA) were used to prepare the small RNA sequencing library. Thereafter, the constructed library was sequenced using Illumina HiSeq2000/2500 with a single-ended read length of 1×50 bp. The analysis results were determined with a significance threshold of $P < 0.05$. The upregulated miRNA statistical map, clustering heat map, and volcano map were generated. Finally, differential miRNA target genes were predicted and subjected to enrichment analysis. Quality control for RNA-seq data was performed using FastQC to assess raw read quality, including base quality scores, GC content, and sequence length distribution. Low-quality reads and adapter sequences were removed using Trimmomatic.

GO and KEGG enrichment analyses were applied to identify significantly differentially expressed GO functional entries and KEGG enrichment pathways. GO and KEGG enrichment analyses were performed using ggplot2 (Version: 3.4.0). The analysis was performed using the “ggplot2” package in R, and proteins exceeding the significance threshold were annotated for further interpretation. The expression of miRNA was displayed using $\log_{10}(\text{norm value})$ ($\log_{10}(0.0001)$ when the norm value is 0). In cases of biological repeats, the norm value of different miRNAs was used for miRNA expression display through the Z-value method. The formula for calculating the Z value is: $Z_{\text{sample-i}} = [(\text{norm sample-i}) - \text{Mean}(\text{norm of all samples})] / [\text{Standard deviation}(\text{norm of all samples})]$.

Olink immuno-oncology assay

Protein levels were measured by multiplex Proximity Extension Assay (PEA) (Olink Proteomic, Uppsala, Sweden) commercial panel (Immuno-Oncology). Olink proteomics relies on PEA technology, enabling the simultaneous analysis of 92 inflammation-related biomarkers. Each target protein was identified using double antibodies and coupled with its specific complementary DNA barcode. The resulting DNA sequences were then detected and quantified using a high-throughput microfluidic real-time PCR instrument (Biomark HD, Fluidigm). The obtained data underwent qualitative control and normalization using internal extension control and interboard control to adjust for in-run and inter-run variations. Proteins with signal intensities below the detection limit or with a signal-to-noise ratio (SNR) < 3 were excluded. Technical replicates were assessed for consistency, with a Pearson correlation coefficient > 0.95 and a coefficient of variation (CV) $< 20\%$ considered acceptable. The quality of the samples was assessed by evaluating the deviation of each sample from the median of the controls. Samples with a deviation of less than 0.3 NPX from the median passed the quality control.

A clustering heatmap analysis was conducted to uncover distinct patterns of protein expression across the

samples. Hierarchical clustering was employed to group proteins and samples based on their similarity. The heatmap was created using the R package “pheatmap” (Version: 1.0.12), with dendrograms included to illustrate the hierarchical relationships between proteins and samples. Volcano plot analysis was used to visually represent the results of the differential protein expression analysis. Receiver Operating Characteristic (ROC) curve analysis was conducted to assess the diagnostic performance of the selected biomarkers. The limma package was employed to identify differentially expressed proteins, with a P-value cutoff of 0.05. The ROC curve was constructed using the “pROC” package in R (Version: 1.18.0), and the optimal cut-off threshold was identified by maximizing Youden’s index.

WGCNA analysis and driver gene mining

Using RNA-seq normalized expression data, a weighted coexpression network was constructed using Weighted gene co-expression network analysis (WGCNA) (version 1.69) with default parameters. Pearson’s correlation coefficient was employed to assess the correlation between gene modules and treatment information within patient groups. Subsequently, hub genes were identified based on the connectivity of gene modules and their association with phenotypic traits within the modules. Module connectivity was defined as the correlation between genes and modules (module membership), while clinical feature relationship was defined as the absolute value of Pearson’s correlation coefficient between each gene and therapeutic information (phenotypic significance). Candidate hub genes were screened based on a module membership degree > 0.6 and phenotypic significance > 0.6 . The final hub gene was determined by selecting the common gene that met both criteria. Signal pathways enriched by hub genes were analyzed using the cluster Profiler package (version 3.14.3).

Immuno-infiltration and miRNA regulatory element

xCell (version 1.1.0) was employed to calculate the proportion of infiltrating immune cells in each sample using RNA-Seq standardized expression data. The miRWalk database was used to extract regulatory outcomes of corresponding target genes exhibiting significant differences in medium and high expression of miRNA results. The Pearson’s correlation coefficient was calculated for proteins between the T1 and T2 groups. Proteins with an absolute correlation coefficient value greater than or equal to 0.5 with target molecules were identified as their co-expressed proteins.

Statistical analysis

Normalized Protein Expression (NPX) values were utilized for analysis as they approximated a normal

distribution. The Olink proteomics final analytical readings are expressed as NPX values, followed by log2 conversion. The volcano plot was generated by plotting the negative logarithm of the p-value ($\log_{10}(\text{p-value})$) on the y-axis and the log-transformed fold change (\log_2 fold change) on the x-axis. Proteins exhibiting statistically significant differential expression ($\text{p-value} < 0.05$) were emphasized. The area under the ROC curve (AUC) was computed to quantify the sensitivity and specificity of the biomarkers in distinguishing between the conditions of interest. An AUC value exceeding 0.7 was deemed indicative of robust diagnostic accuracy, with values approaching 1 reflecting superior discriminatory capability. Data are presented as mean \pm standard deviation or median (first and third quartiles). Statistical analysis was performed using SPSS Statistics 25.

The Wilcoxon rank-sum test was used to compare the significance of differences in the proportion of infiltrated immune cells between groups. Survival analysis of the different group was performed using the Kaplan-Meier method. Statistically significant difference in the two groups was then defined by a log-rank test (Mantel Cox, 95% CI) of the Kaplan-Meier curves. A P -value < 0.05 was considered statistically significant.

Results

Characteristics of the participants

Sixteen patients who met the inclusion criteria participated in this study, and the experimental flowchart

is shown in Fig. 1. As the study design, plasma samples from all 16 enrolled patients were selected for Olink proteomics analysis, of which nine patients underwent leukocyte RNA-seq. A comparison was made between the data obtained before and after the first neoadjuvant therapy. The patient characteristics are detailed in Table 1. Within this cohort, TRG is a measure of histopathological response to neoadjuvant therapy, patients in the T1 group comprised those with TRG0 and TRG1, while those in the T2 group included patients with TRG2 and TRG3.

Enrichment of tumor immune-related inflammatory pathways

We conducted a correlation analysis of tumor-infiltrating immune cells in the T1 and T2 groups (Fig. 2A). The results revealed that, compared with the T1 group, CD8^+ T cells and B cells in the T2 group significantly decreased, while monocytes and neutrophils significantly increased. To elucidate the infiltration of immune cells in vivo with the treatment, we further analyzed the T1 and T2 groups before and after neoadjuvant therapy, respectively. We found that in the T1 group, CD4^+ T cells and monocytes were higher after treatment than before treatment. The number of CD8^+ T cells increased and the number of B cells decreased in T2 group after treatment compared with before treatment. Overall, compared with the T1 group, the number of B cells decreased, and the number of neutrophils increased in the T2 group, as

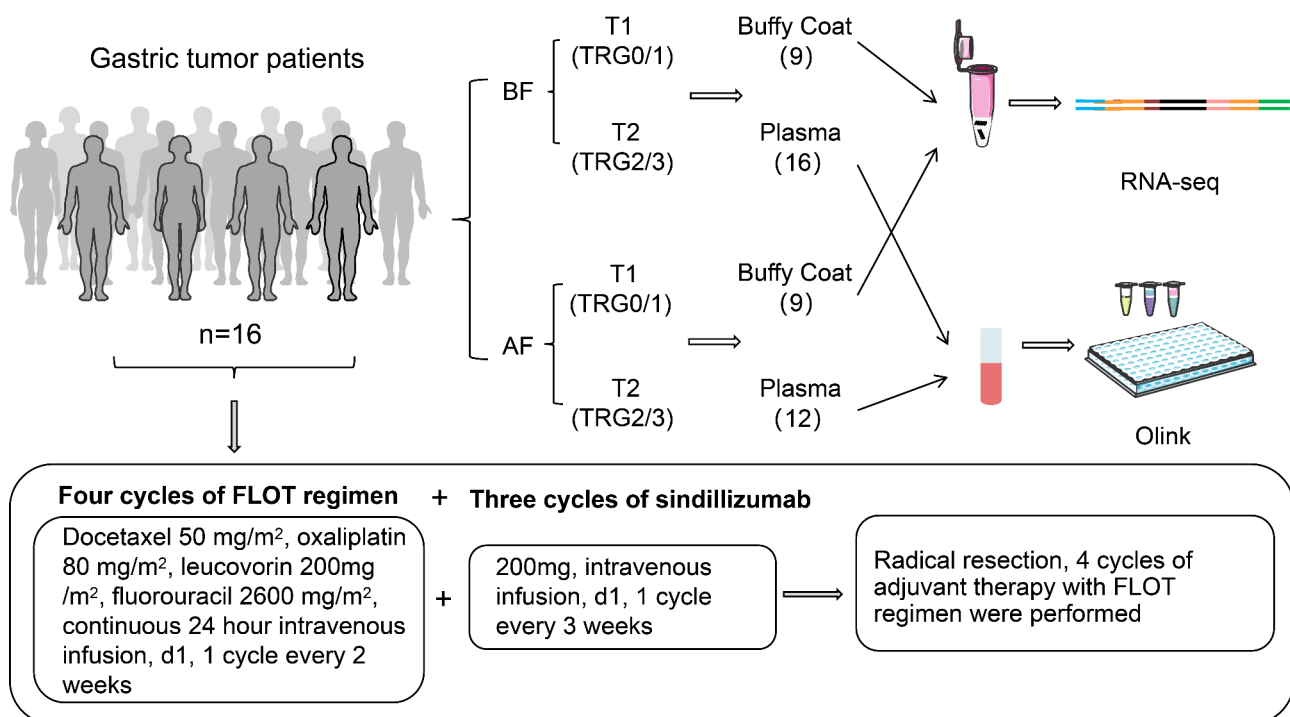


Fig. 1 Schematic of experimental workflow. BF: Before Treatment, AF: After Treatment

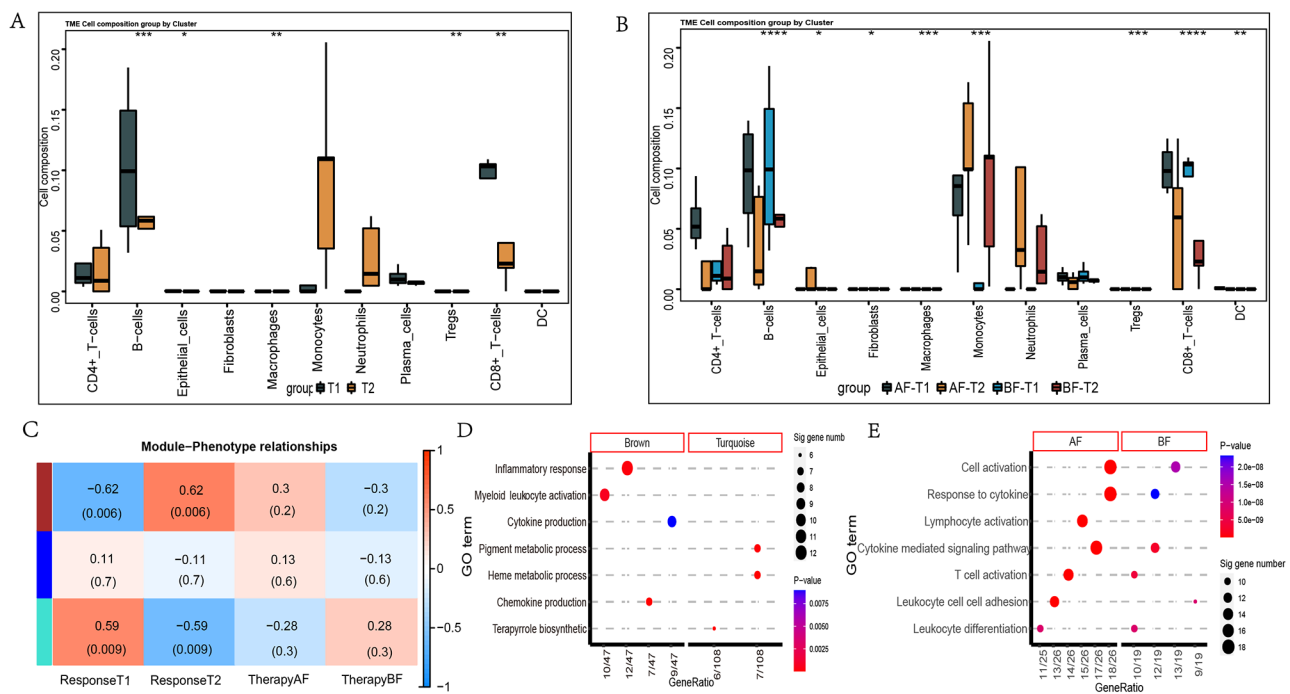


Fig. 2 The analysis of protein expression and related signaling pathways in different groups. **(A)** Relationship between total T1 and T2 expression and proportion of immune cells. **(B)** Relationship between expression and proportion of immune cells in T1 and T2 groups before and after treatment. **(C)** WGCNA results show the gene modules in distinct treatment response phenotype. Columns represent treatment response phenotype. The color change from blue to red indicates a low to high correlation between gene module and cell subtypes (Pearson's correlation test). **(D)** Dot plot showing the GO enrichment analysis results using the hub genes in different response groups. Colors from blue to red indicate the $\text{Log}_{10}(P\text{-value} + 1)$ low to high (clusterProfiler). **(E)** GO enrichment analysis based on the background of 92 inflammation-related proteins. BF: Before Treatment, AF: After Treatment

shown in Fig. 2B. In addition, we employed complementary approaches, including TIMER, CIBERSORT, and Consensus methods (Supplementary Fig. 1). The results derived from these methods were consistent with the xCell analysis, demonstrating comparable CD8+ T cell enrichment patterns.

Based on miRNA data, the highest enrichment scores for the T1 and T2 groups were 0.59 ($P=0.009$) and 0.62 ($P=0.006$), respectively (Fig. 2C). GO enrichment analysis was conducted on the expression of significantly different genes in the respective groups. The pathways associated with inflammatory response and myeloid leukocyte activation exhibited the most significant differences (Fig. 2D). To further investigate the function of differentially expressed proteins, we conducted GO enrichment analysis in different contexts. The results revealed that the differential proteins were enriched in cell activation, response to cytokine, the cytokine-mediated signaling pathway, and T cell activation, lymphocyte activation was enriched after treatment but not before treatment (Fig. 2E).

Upon analyzing RNA-seq data, the inflammatory pathway emerged as the most significantly different in the T1 and T2 groups. Furthermore, we analyzed the expression of 92 proteins related to tumor immunity in different groups using Olink proteomics. GO and Kyoto

Encyclopedia of Genes and Genomes (KEGG) enrichment analysis showed that these proteins were enriched in various inflammatory responses, immune responses and chemokine activities (Fig. 3A), with several pathways, such as the cytokine-cytokine receptor interaction, chemokine signaling pathway, and TNF signaling pathway (Fig. 3B).

Key molecular biomarkers were associated with immune infiltration

Pearson's correlation analysis revealed the interaction of 57 proteins after treatment (Supplementary Fig. 2). Seven related proteins with the most noticeable differences were identified between the T1 and the T2 group, including Angiopoietin 2 (ANGPT2), PGE, C-X3-C motif chemokine ligand 1 (CX3CL1), TNFRSF21, C-X-C motif chemokine ligand 10 (CXCL10), C-X-C motif chemokine ligand 9 (CXCL9), and Granzyme B (GZMB). Compared to the T2 group, these seven different proteins were significantly downregulated in the T1 group (Fig. 4A-B). ROC curve results demonstrated that the AUC of PGE, IL33, TNFRSF21, IL15, and IFN-gamma were all >0.8 , the AUC values of PGF was 0.9143 (Fig. 4C). To further observe the potential role of the related molecules, we analyzed the data of 12 patients before and after neoadjuvant therapy (Fig. 4D). The results revealed that

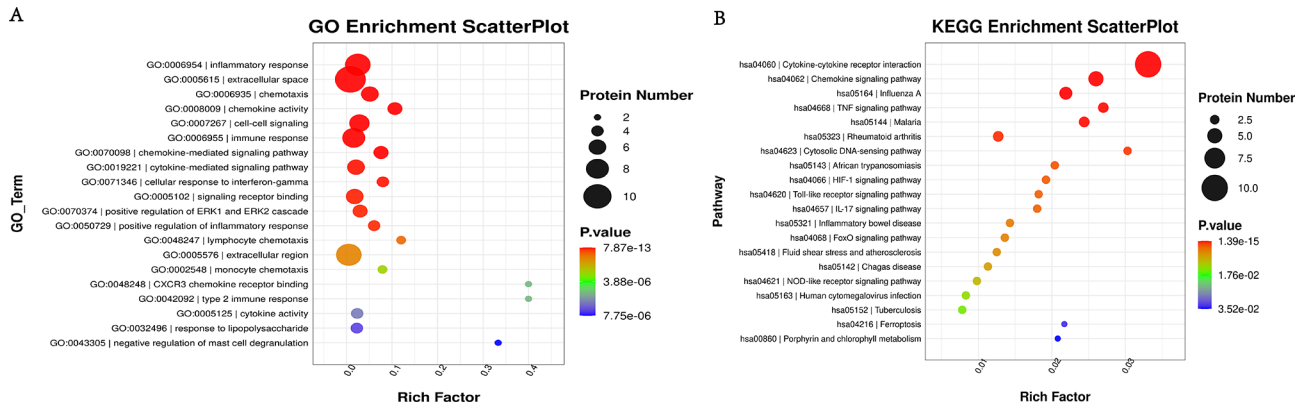


Fig. 3 Olink proteomic analysis of tumor immune-related proteins. **(A)** GO enrichment analysis based on the background of all annotated proteins. **(B)** KEGG enrichment analysis based on the background of all annotated proteins

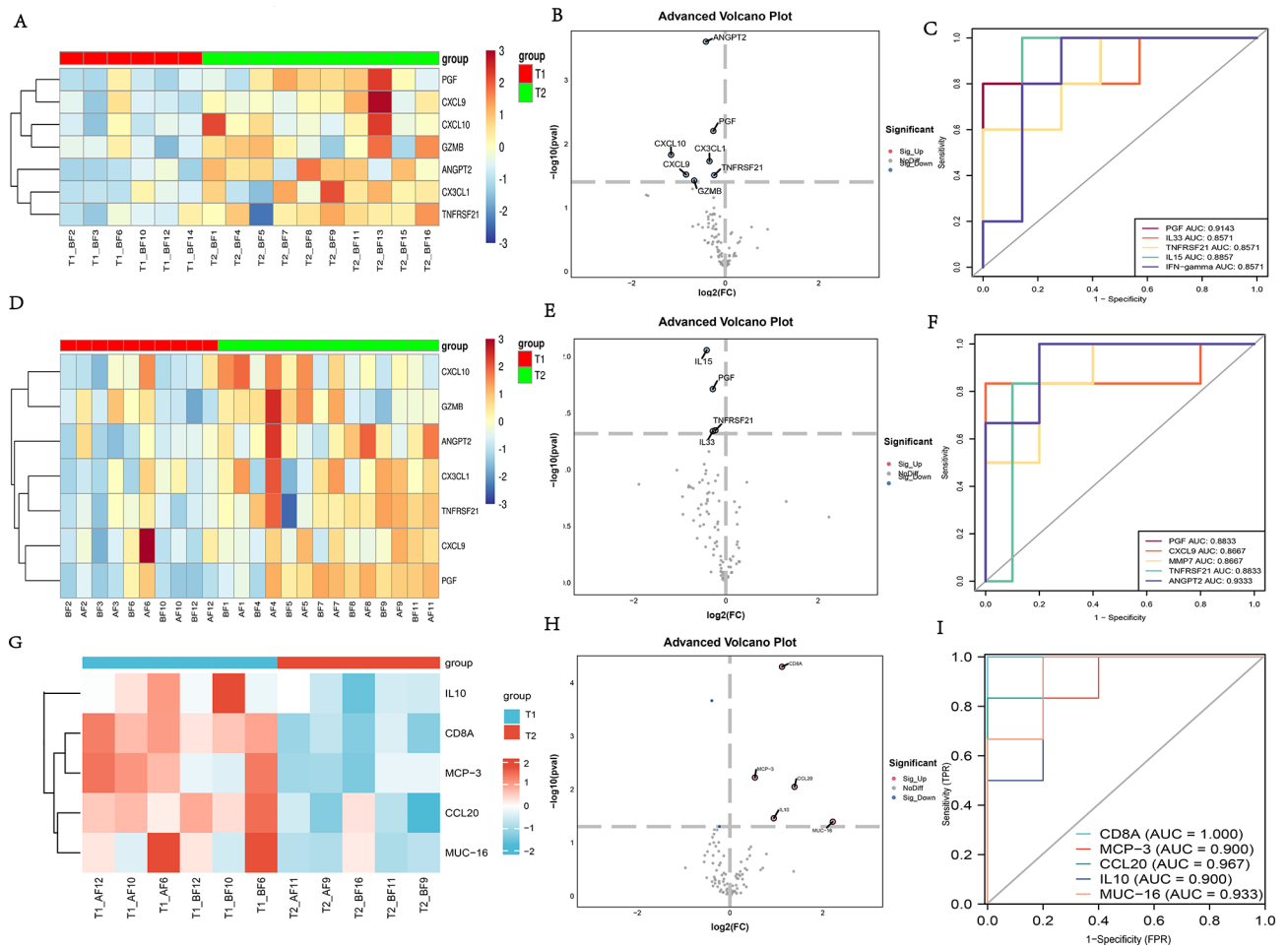


Fig. 4 Differential protein biomarkers associated with inflammation between the T1 and T2 groups. **(A)** Heatmaps of seven differentially expressed proteins in T1 and T2 groups before treatment. **(B)** Volcanic visualization of seven inflammation-related biomarkers in T1 and T2 groups before treatment. **(C)** ROC plots in T1 and T2 groups before treatment (PGF, IL33, TNFRSF21, IL15, and IFN- γ). **(D)** Heatmap of seven differentially expressed proteins before treatment (BF) and after treatment (AF). **(E)** Volcanic visualization of seven inflammation-related biomarkers in T1 and T2 groups after treatment. **(F)** ROC plots in T1 and T2 groups after treatment (PGF, CXCL9, MMP7, TNFRSF21, and ANGPT2). **(G)** Heatmaps of five differentially expressed proteins in T1 and T2 groups before and after treatment. **(H)** Volcanic visualization of five inflammation-related biomarkers in T1 and T2 groups. **(I)** ROC curves of T1 and T2 groups before and after treatment (CD8A, MCP-3, CCL20, IL10, MUC-16). BF: Before Treatment, AF: After Treatment

compared with before treatment, some proteins such as TNFRSF21 and PGF were also highly expressed after treatment. Figure 4E–F shows the volcano maps and ROC curves of the T1 and T2 groups after neoadjuvant therapy, wherein the Area under curve (AUC) values of TNFRSF21 and PGF were both 0.8833. Further cluster analysis was conducted on relevant differential proteins in the T1 and T2 groups before and after neoadjuvant therapy. The results indicated that compared with the T1 group, the CD8A protein expressions in the T2 group were decreased, the AUC values of the top three were CD8A(1.000), CCL20(0.967), and MUC-16(0.933) respectively (Fig. 4G–I).

These pathways may be linked to neoadjuvant therapy and prognosis in different groups. Simultaneously, heatmaps were generated for the relevant mRNA of samples from the T1 and T2 groups before neoadjuvant therapy, revealing 68 differentially expressed inflammation-related genes between them. Among these, 50 differentially expressed genes were downregulated in the T2 group compared to the T1 group, while 18 genes, including hsa-let-7f-2-3p_1ss22CT, hsa-miR-3665-p5_1ss17AG, mmu-miR-5126_L-1_1ss18CTI, were upregulated. Notably, hsa-miR-1278_R-2, hsa-miR-548aa-1-p3_1ss19TG, and hsa-miR-125b-5p_R-1 were also included (Supplementary Fig. 3A). A volcano map was generated to visualize the overall distribution of different miRNAs (Supplementary Fig. 3D). Additionally, differences in CircRNA and LncRNA were analyzed in the T1 group (No.3, No.6, No.10, No.12) and T2 group (No.1, No.7, No.9, No.13, No.16). Compared with the T1 group, the most significantly increased circRNA was circRNA15735, and the most decreased was hsa_circ_0007313 in the T2 group (Supplementary Fig. 3B–C, E–F).

Expression and prognostic value of CD8A and PGF in gastric cancer

Box plots were generated to describe the expression of two different prognostic proteins in the T1 and T2 groups (Figs. 5A–B), the expression of CD8A in T1 group was significantly higher than that in T2 group, while the expression level of PGF in T2 group was significantly increased. The prognostic value of differentially expressed genes in gastric cancer was assessed through Kaplan–Meier survival analysis, using complete mRNA transcriptomics data from The Cancer Genome Atlas (TCGA). It showed that high expressions of CD8A was associated with a favorable prognosis in patients with gastric cancer, with logrank P -value < 0.05 (Fig. 5C). Conversely, high expression of PGF was associated with a poor prognosis in patients with gastric cancer, with logrank P -value < 0.05 (Fig. 5D).

Analysis of Immunoinfiltration and interaction between CD8 and PGF

Figure 6A–B illustrates the coexpression network before and after treatment. Proteins associated with CD8A and PGF before treatment included IL8, CX3CL1, GZMH, VEGFA, TNF, and CCL3. After treatment, the proteins associated with both were TNF, IL15, TNFRSF12A, MMP12, HGF, CX3CL1 and IL18. Three proteins, TNF, CX3CL1 and IL8, were involved both before and after treatment. CD8A was positively correlated with monocytes, macrophages, TNK cells, CD8 cells, dendritic cells, and negatively correlated with MDSC, while PGF was positively correlated with MDSC and TNK cells (Fig. 6C). In addition, miRNAs with medium and high expression levels were selected and the regulatory results of corresponding target genes were analyzed through miRWalk database mining (Fig. 6D).

Discussion

Analyzing protein expression in peripheral blood offers a minimally invasive and accessible approach for monitoring biomarkers during neoadjuvant immunotherapy. Tumor biomarker levels play a crucial role in detecting disease recurrence in cancer patients. Established biomarkers, including PSA, CEA, CA19-9, and CA72-4, are routinely utilized to assess the recurrence of gastric cancer [13, 14]. However, there are few indicators that can predict the efficacy of neoadjuvant therapy for gastric cancer. To our knowledge, this is the first study analyzing changes in plasma protein levels before and after neoadjuvant immunotherapy for gastric cancer. We identified two potential markers with distinct prognostic significance within the gastric cancer immunotherapy neoadjuvant clinical trial cohort. Notably, CD8A exhibited increased expression in the T1 group after neoadjuvant therapy and were positively correlated with the efficacy of immunoinfiltrating cells, including monocytes, macrophages, TNK cells, CD8 cells. Conversely, the expression of PGF demonstrated significant increased in the T2 group, correlating with the tumor regression grade of neoadjuvant therapy.

CD8A, a member of the T cytotoxic pathway-related genes, encodes the CD8 antigen, a cell surface glycoprotein found on most cytotoxic T cells. The CD8 antigen functions as a coreceptor with the T-cell receptor, facilitating the recognition of antigens presented by antigen-presenting cells in the context of class I MHC molecules. CD8A expression may be a useful and measurable predictive marker of immunotherapeutic response and immune cell infiltration [15]. A previous study for pan-cancer has reported that high level of CD8A in conjunction with high expression of PD-L1 might be used to predict the immunotherapeutic response [16]. Previous studies also revealed the protective role of CD8A in the prognoses of

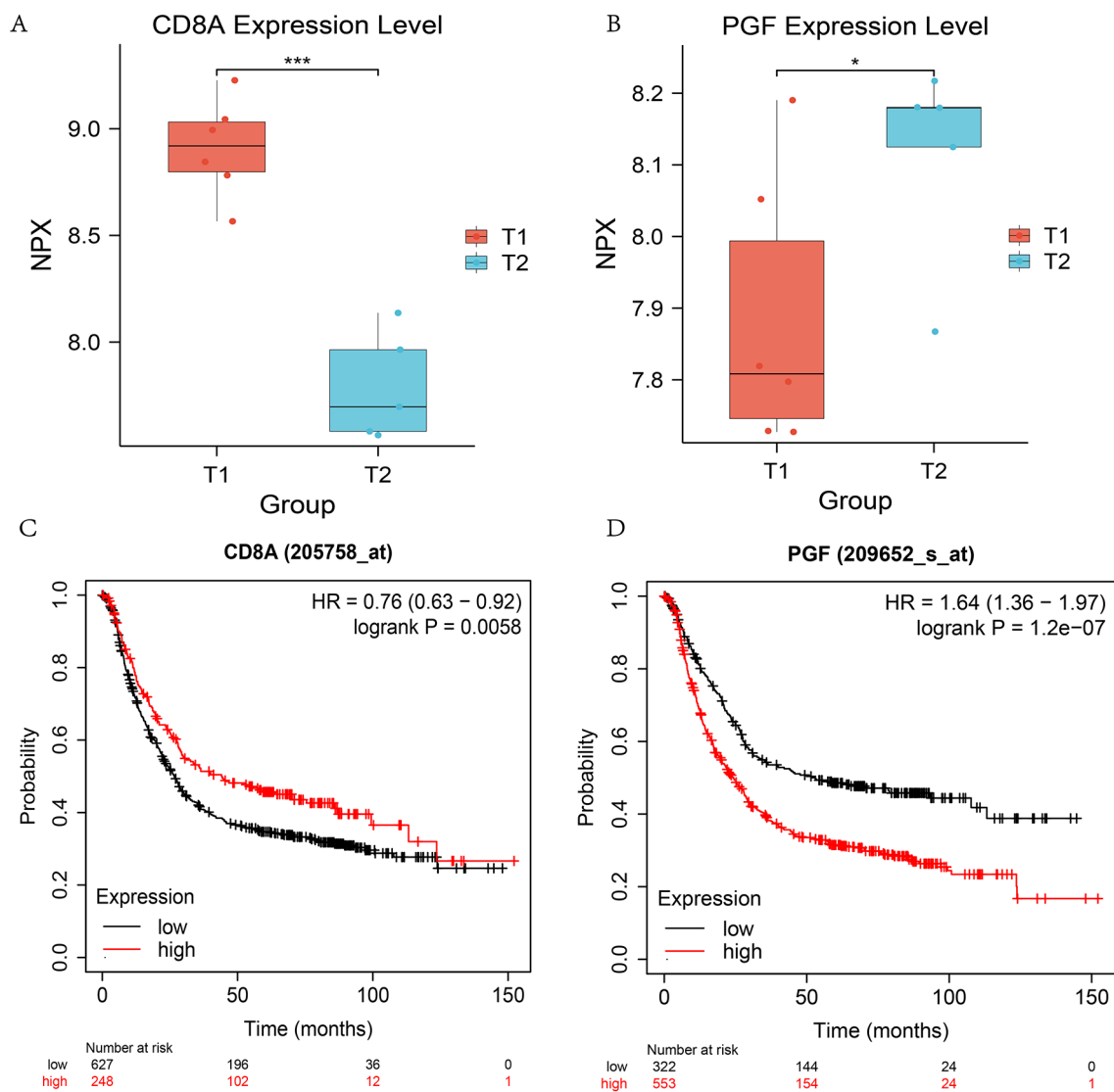


Fig. 5 Biomarkers of different proteins associated with T1 and T2 groups. **(A–B)** Expression of CD8A and PGF protein in T1 and T2 groups. **(C–D)** Kaplan-Meier survival analysis was used to evaluate the prognostic value of differentially expressed genes in CD8A and PGF

hepatocellular carcinoma, metastatic melanoma, head / neck squamous cell carcinoma and bladder carcinoma [17–19]. However, few studies have clarified the association between CD8A and immunotherapeutic response in gastric cancer. Therefore, we further investigated the prognostic value of CD8A in cancer patients treated with immunotherapy in TCGA dataset. Our results showed that low CD8A expression was associated with poor survival outcomes among cancer patients treated with immunotherapy. Thus, CD8A can serve not only a useful prognostic factor in gastric cancer patients but also a predictive marker of immunotherapeutic response in cancer patients treated with immunotherapy.

A growing body of evidence suggested the involvement of growth factors in the development of various malignancies, including gastric cancer [20–22]. Growth factors

and their receptors, cell-cycle regulators, cell-adhesion molecules and matrix-degrading enzymes are those to be used as prognostic factors, including epidermal growth factor (EGF), EGF receptor, vascular endothelial growth factor (VEGF), et al. [22]. Such as c-type lectin domain family 11 member A (CLEC11A), have been identified as potential prognostic and immunological biomarkers in gastric cancer, playing a significant role in tumor progression, modulation of the immune microenvironment, and therapeutic response, thereby providing valuable insights for the development of personalized treatment strategies [23]. PGF is well known as a member of the VEGF family, which is active in angiogenesis and endothelial cell growth, exerting an effect on its proliferation and migration. PGF has been reported as a potent stimulator in cancer invasion by activating angiogenesis [24].

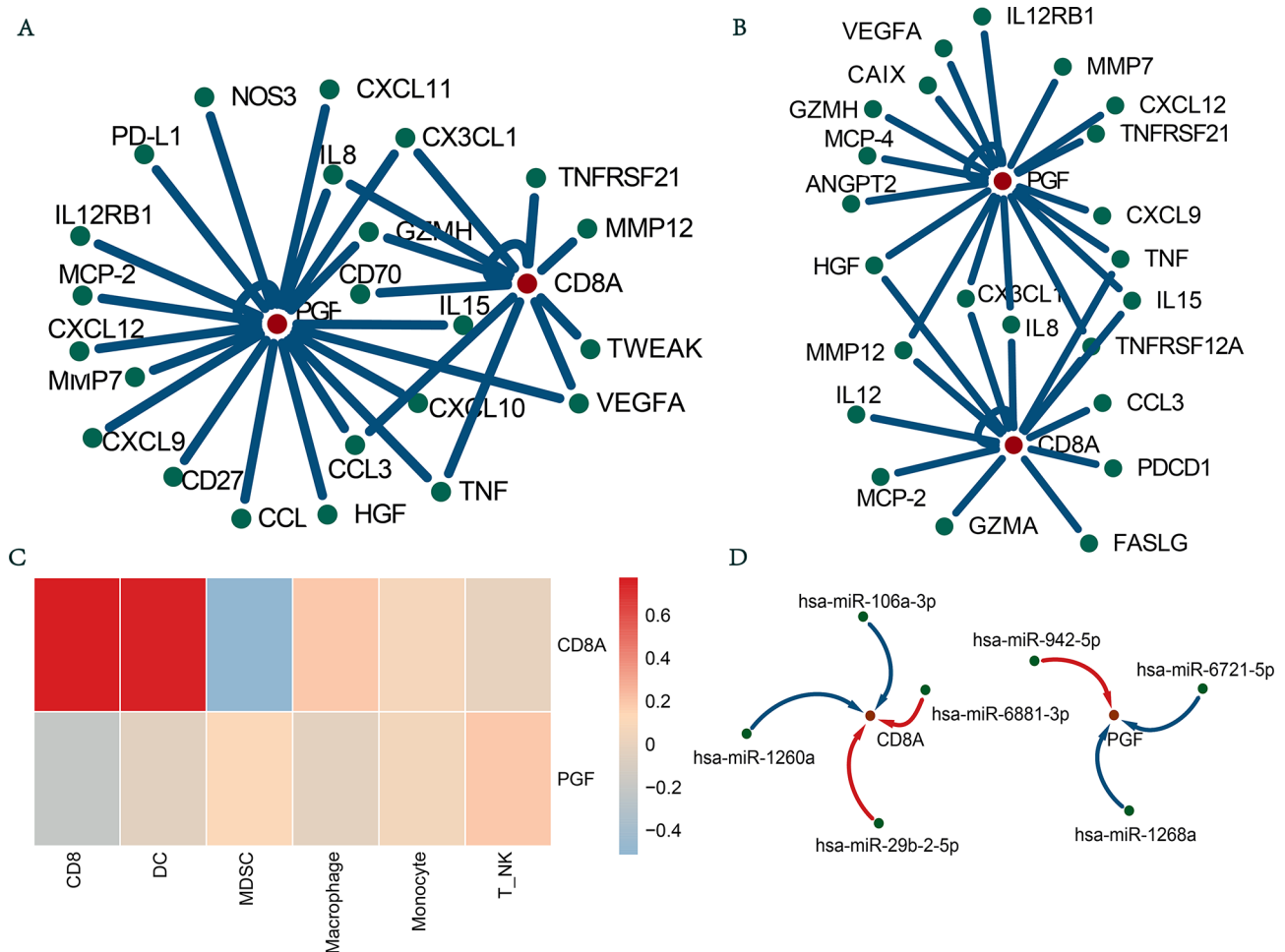


Fig. 6 Mechanism analysis of CD8A and PGF. **(A–B)** Gene coexpression network analysis of the inflammation-related differentially expressed proteins. **(C)** Heatmap of the correlation between the expression of four response-favorable genes and immune cells using the expression data in TCGA. **(D)** Network illustrates the potential miRNA-regulated networks associated with four response-favorable genes. Genes are represented by red dots and miRNAs are represented by green dots. The blue line indicates the inhibitory relationship between the miRNA and its target gene, while the red line indicates the promoting relationship

In addition, the overexpression of PGF is correlated with tumor stage, cancer progression and metastasis [25–27]. In colorectal cancer, Kaplan–Meier curve analysis has showed that higher expression of the PGF gene is associated with a lower survival rate, and in vitro expression of PGF aligns with bioinformatics results [28]. Our study similarly found that PGF was markedly overexpressed in gastric cancer, functioning as a molecule with oncogenic properties.

Our study revealed that, CD4⁺T cells and monocytes increased in the T1 group after treatment, while CD8⁺T cells and B cells decreased in the T2 group after treatment. The use of immune cell infiltration as a novel biomarker for predicting the prognosis of patients with various types of cancer holds great promise [29, 30]. While previous reports have implicated immune infiltration in affecting tumor patient prognosis [31–33], the interaction mechanism between prognosis and the

tumor microenvironment remains incompletely understood. Neutrophils play a pivotal role in tumor formation and metastasis, exhibiting a dual role in inhibiting and promoting cancer [34, 35]. The mechanism of cancer progression is intricately linked to inflammation. Our evaluation of immune cell expression in different tumor microenvironments revealed higher expression levels of monocytes and neutrophils in the T2 group compared to the T1 group. Additionally, the infiltration of CD8⁺T cells, NK cells, and B cells was lower in the T2 group, whereas memory CD4⁺T cells increased in both groups. Elevated leukocyte levels in the blood significantly correlate with short survival and cancer cell metastasis in patients with non-hematologic malignancies, primarily attributed to an increase in mature polymorphonuclear cells [36]. B cells play a crucial role in humoral immunity, inhibiting the progression of tumor cells by secreting immunoglobulin and promoting T cell responses [37,

38]. The heightened presence of inflammatory cells can induce the production and secretion of various chemokines and cytokines, serving as inflammatory mediators that recruit more inflammatory cells to the tumor microenvironment, thereby exacerbating a vicious cycle.

Based on existing research, gastric cancer patients with high CD8A expression may demonstrate increased sensitivity to PD-1 inhibitors [39]. PGF plays a crucial role in tumor angiogenesis and immune suppression [40–42]. This study reveals that elevated PGF expression correlates with poor prognosis in gastric cancer patients, suggesting its potential as a therapeutic target for anti-angiogenic treatment. Future investigations could explore the relationship between PGF expression levels and the efficacy of anti-angiogenic therapies, thereby offering more precise treatment options for gastric cancer patients. Furthermore, the combination of CD8A and PGF may provide a more comprehensive prognostic assessment and therapeutic guidance for gastric cancer patients. By integrating genomic, transcriptomic, and proteomic data, further exploration of the interactions between CD8A, PGF, and other molecular markers could facilitate the development of more accurate predictive models. In the future, prospective clinical trials based on CD8A and PGF expression levels could be designed to evaluate their predictive value in gastric cancer immunotherapy, anti-angiogenic therapy, or combination therapies. Additionally, CD8A, as a universal marker of T cell activity, may also possess predictive value in other immunotherapy-sensitive cancer types, such as melanoma [43], non-small cell lung cancer [44], and colorectal cancer [45]. PGF is associated with angiogenesis and tumor progression in various solid tumors, including breast cancer [46], liver cancer [47], and pancreatic cancer [24]. Consequently, PGF may serve as a pan-cancer prognostic marker and therapeutic target.

To facilitate the broader clinical application and validation of CD8A and PGF, we will develop standardized ELISA detection methods. Utilizing the Human ELISA Kit, we aim to measure the expression levels of CD8A and PGF both prior to and following neoadjuvant therapy. Furthermore, we will rigorously assess the stability and reproducibility of these biomarkers across various gastric cancer subtypes. According to the results of this study, when treated with neoadjuvant immunotherapy using sintilimab in combination with FLOT protocol of gastric cancer patients, we can detect the expression levels of CD8A and PGF before and after neoadjuvant therapy. This approach facilitates the assessment and prediction of potential therapeutic responses. Furthermore, it is recommended to establish a systematic protocol for post-treatment blood monitoring (e.g., at 3–6 month intervals) to enhance the predictive capacity for disease progression.

The present study has some limitations. First, we did not sequence tissue samples in the tumor microenvironment, which will require additional mechanistic analysis in the future. Second, the number of gastric/gastroesophageal samples in our center is limited. It is necessary to increase the healthy control group, and a larger cohort of gastric adenocarcinoma patients with control group, pre- and post-operative RNA sequences need to be collected to further evaluate the performance of gastric adenocarcinoma models in predicting the expression of these molecules. In future studies, we will employ multivariate analysis or stratified analysis to control for confounding factors such as age, gender, lifestyle habits, and comorbidities, thereby further ensuring the stability and broader applicability of the current results.

Conclusions

Our study conducted a comprehensive assessment of potential carcinogenic pathways, revealing novel associations related to the diagnosis and prognosis of gastric and gastroesophageal cancers. Our data suggest that neoadjuvant therapy efficacy may be reflected by alterations in specific proteins, offering potential etiological and clinical implications. The molecular aspects of tumor regression after neoadjuvant chemotherapy are currently under investigation, and our findings indicate that the promising candidate markers CD8A and PGF are strongly associated with immune invasion, potentially providing novel treatment strategies for patients with gastric adenocarcinoma.

Abbreviations

WGCA	Weighted gene co-expression network analysis
TRG	Tumor Regression Grade
ROC	Receiver Operating Characteristic
CD8A	CD8a molecule
CCL20	C motif chemokine ligand 20
PGF	Placenta Growth Factor
TNFRSF21	TNF receptor superfamily member 21
DC	Dendritic Cell
MDSC	Myeloid-derived suppressor cell
OS	Overall survival
PFS	Progression-free survival
EFS	Event-free survival
pCR	Pathological complete response
PD-L1	Programmed cell death-Ligand 1
CPS	Combined Positive Score
FLOT	Fluorouracil, Leucovorin, Oxaliplatin, and Docetaxel
KEGG	Kyoto Encyclopedia of Genes and Genomes
ANGPT2	Angiopoietin 2
CX3CL1	C-X ₃ -C motif chemokine ligand 1
CXCL10	C-X-C motif chemokine ligand 10
CXCL9	C-X-C motif chemokine ligand 9
GZMB	Granzyme B
AUC	Area under curve

Supplementary Information

The online version contains supplementary material available at <https://doi.org/10.1186/s12885-025-14046-7>.

Supplementary Material 1: Supplementary Fig.1 Relationship between expression and proportion of immune cells in T1 and T2 groups before and after treatment. A: TIMER, B: CIBERSORT, C: onsensus.

Supplementary Material 2: Supplementary Fig.2 Correlations between the differentially expressed inflammation-related biomarkers in after treatment (AF).

Supplementary Material 3: Supplementary Fig.3 The difference of MiRNA, LncRNA, and CircRNA in T1 and T2 groups.

Acknowledgements

The authors express their gratitude to all of the participants in the study.

Author contributions

Chengjuan Zhang conceived and participated in research design, article writing. Tingjie Wang contributed to bioinformatic analysis. Jing Yuan performed the image arrangement and drafted the manuscript. Tao Wang and Bin Ma supervised the experiments and revised the manuscript. Benling Xu contributed to clinical sample collection, Ruihua Bai, Xiance Tang and Xiaojie Zhang contributed to confirmation of pathological information. Mingqing Wu, Tianqi Lei, Wenhao Xu were responsible for sample processing and storage. Yongjun Guo conceived the study, Ning Li conceived the study and provided clinical samples. All authors read and approved the final manuscript.

Funding

This research was supported by the Major public welfare projects in Henan Province- Research and development of new technologies for tumor liquid biopsy and immunotherapy (201300310400), The Health Science and Technology Innovation Project for Young people of Henan Provincial (YXKC2021032, YXKC2021008), Zhengzhou University Young Teachers Basic Research Training Project (JC23858081), Natural Science Foundation of Henan Province Project (242300420095). Henan Province and Ministry of Health of Medical Science and Technology (SBGJ202302028).

Data availability

The datasets generated and analysed during the current study are available in the GSA repository, number of BioProject is PRJCA025579 (<https://ngdc.cnbcba.c.cn/gsa-human/s/YttfTn11>).

Declarations

Ethics approval and consent to participate

This study was conducted in accordance with the Declaration of Helsinki and received approval from the Ethics Committee of Henan Cancer Hospital (Ethics Approval No: 2019214). Written informed consent was obtained from all participants involved in the research.

Consent for publication

Not applicable.

Competing interests

The authors declare no competing interests.

Author details

¹Center of Bio-Repository, The Affiliated Cancer Hospital of Zhengzhou University, Henan Cancer Hospital, Zhengzhou, China

²Department of Molecular Pathology, The Affiliated Cancer Hospital of Zhengzhou University, Henan Cancer Hospital, Zhengzhou, China

³Henan Key Laboratory of Molecular Pathology, Zhengzhou, Henan, P. R. China

⁴The Kids Research Institute Australia, School of Medicine, the University of Western Australia, Nedlands, WA, Australia

⁵School of Medical, Molecular and Forensic Sciences, Murdoch University, Murdoch, WA, Australia

⁶Department of Immunotherapy, The Affiliated Cancer Hospital of Zhengzhou University, Henan Cancer Hospital, Zhengzhou, China

⁷Department of Pathology, The Affiliated Cancer Hospital of Zhengzhou University, Henan Cancer Hospital, Zhengzhou, China

⁸Department of Medical Records, The Affiliated Cancer Hospital of Zhengzhou University, Henan Cancer Hospital, Zhengzhou, China

⁹Department of Oncology, The Affiliated Cancer Hospital of Zhengzhou University, Henan Cancer Hospital, Zhengzhou, China

Received: 29 August 2024 / Accepted: 31 March 2025

Published online: 12 April 2025

References

- Sung H, Ferlay J, Siegel RL et al. Global Cancer Statistics 2020: GLOBOCAN Estimates of Incidence and Mortality Worldwide for 36 Cancers in 185 Countries. *CA Cancer J Clin.* 71(3). United States:Wiley-Blackwell,2021. 209–249.
- Thrift AP, El-Serag HB. Burden of Gastric Cancer. *Clin Gastroenterol Hepatol.* 18(3). United States:W.B. Saunders Ltd,2020. 534–542.
- Ham IH, Oh HJ, Jin H et al. Targeting interleukin-6 as a strategy to overcome stroma-induced resistance to chemotherapy in gastric cancer. *Mol Cancer.* 18(1). England:BioMed Central,2019. 68.
- Wagner AD, Syn NL, Moehler M et al. Chemotherapy for advanced gastric cancer. *Cochrane Database Syst Rev.* 8(8). England:other,2017. CD004064.
- Li P, Huang CM, Zheng CH et al. Comparison of gastric cancer survival after R0 resection in the US and China. *J Surg Oncol* 118(6). United States:Wiley-Liss Inc,2018. 975–82.
- Shitara K, Ajani JA, Moehler M et al. Nivolumab plus chemotherapy or ipilimumab in gastro-oesophageal cancer. *Nature.* 603(7903). England:Springer Nature,2022. 942–948.
- Li N, Li Z, Fu Q et al. Efficacy and safety of neoadjuvant sintilimab in combination with FLOT chemotherapy in patients with HER2-negative locally advanced gastric or gastroesophageal junction adenocarcinoma: an investigator-initiated, single-arm, open-label, phase II study. *Int J Surg* 110(4). United States:other,2024. 2071–2084.
- Park JE, Kim SE, Keam B et al. Anti-tumor effects of NK cells and anti-PD-L1 antibody with antibody-dependent cellular cytotoxicity in PD-L1-positive cancer cell lines. *J Immunother Cancer.* 8(2). England:BioMed Central,2020. e000873.
- Xing X, Guo J, Ding G et al. Analysis of PD1, PDL1, PDL2 expression and T cells infiltration in 1014 gastric cancer patients. *Oncoimmunology* 7(3). United States:Landes Bioscience,2018. e1356144.
- Dong W, Wu X, Ma S et al. The Mechanism of Anti-PD-L1 Antibody Efficacy against PD-L1-Negative Tumors Identifies NK Cells Expressing PD-L1 as a Cytolytic Effector. *Cancer Discov.* 9(10). United States:American Association for Cancer Research Inc,2019. 1422–1437.
- Glickman JW, Dubin C, Renert-Yuval Y et al. Cross-sectional study of blood biomarkers of patients with moderate to severe alopecia areata reveals systemic immune and cardiovascular biomarker dysregulation. *J Am Acad Dermatol* 84(2). United States:Mosby Inc,2021. 370–80.
- Yao P, Iona A, Pozarickij A et al. Proteomic analyses in diverse populations improved risk prediction and identified new drug targets for type 2 diabetes. *Diabetes Care* 47(6). United States:American Diabetes Association Inc,2024. 1012–9.
- Kim DH, Oh SJ, Oh CA et al. The relationships between perioperative CEA, CA 19–9, and CA 72–4 and recurrence in gastric cancer patients after curative radical gastrectomy. *J Surg Oncol* 104(6). United States:Wiley-Liss Inc,2011. 585–91.
- Zhou Y, Tao L, Qiu J et al. Tumor biomarkers for diagnosis, prognosis and targeted therapy. *Signal Transduct Target Ther* 9(1). England:Springer Nature,2024. 132.
- Ahmadzadeh M, Johnson LA, Heemskerk B et al. Tumor antigen-specific CD8 T cells infiltrating the tumor express high levels of PD-1 and are functionally impaired. *Blood* 114(8). United States:American Society of Hematology,2009. 1537–44.
- Ock CY, Keam B, Kim S et al. Pan-Cancer Immunogenomic perspective on the tumor microenvironment based on PD-L1 and CD8 T-Cell infiltration. *Clin Cancer Res* 22(9). United States:American Association for Cancer Research Inc,2016. 2261–70.
- Xu D, Liu X, Wang Y et al. Identification of immune subtypes and prognosis of hepatocellular carcinoma based on immune checkpoint gene expression profile. *Biomed Pharmacother.* 126France:other,2020. 109903.
- Lecerf C, Kamal M, Vacher S et al. Immune gene expression in head and neck squamous cell carcinoma patients. *Eur J Cancer.* 121England:other,2019. 210–223.

19. Zheng Z, Guo Y, Huang X, et al. CD8A as a prognostic and immunotherapy predictive biomarker can be evaluated by MRI radiomics features in bladder cancer. *Cancers (Basel)*. 2022;14(19):4866. Switzerland:MDPI (Basel, Switzerland),.
20. Crociani O, Lastraioli E, Boni L et al. hERG1 channels regulate VEGF-A secretion in human gastric cancer: clinicopathological correlations and therapeutical implications. *Clin Cancer Res*. 20(6). United States:American Association for Cancer Research Inc,2014. 1502-12.
21. Guan WL, He Y, Xu RH. Gastric cancer treatment: recent progress and future perspectives. *J Hematol Oncol*. 16(1). England:BioMed Central,2023. 57.
22. Yasui W, Oue N, Aung PP et al. Molecular-pathological prognostic factors of gastric cancer: a review. *Gastric Cancer*. 8(2). Japan:Springer Singapore,2005. 86–94.
23. Zheng Q, Gong Z, Li B et al. Identification and characterization of CLEC11A and its derived immune signature in gastric cancer. *Front Immunol*. 15Switzerland:Frontiers Media S.A,2024. 1324959.
24. Göhrig A, Hilfenhaus G, Rosseck F et al. Placental growth factor promotes neural invasion and predicts disease prognosis in resectable pancreatic cancer. *J Exp Clin Cancer Res* 43(1). England:BioMed Central,2024. 153.
25. Snuderl M, Batista A, Kirkpatrick ND et al. Targeting placental growth factor/neuropilin 1 pathway inhibits growth and spread of Medulloblastoma. *Cell* 152(5). United States:Cell Press,2013. 1065–76.
26. Heindryckx F, Coulon S, Terrie E et al. The placental growth factor as a target against hepatocellular carcinoma in a diethylnitrosamine-induced mouse model. *J Hepatol*. 58(2). Netherlands:Elsevier,2013. 319–28.
27. Wei SC, Tsao PN, Yu SC et al. Placenta growth factor expression is correlated with survival of patients with colorectal cancer. *Gut* 54(5). England:BMJ Publishing Group,2005. 666–72.
28. Shen Y, Ni S, Li S et al. Role of stemness-related genes TIMP1, PGF, and SNAI1 in the prognosis of colorectal cancer through single-cell RNA-seq. *Cancer Med*. 12(10). United States:John Wiley and Sons Ltd,2023. 11611–11623.
29. Mao X, Xu J, Wang W et al. Crosstalk between cancer-associated fibroblasts and immune cells in the tumor microenvironment: new findings and future perspectives. *Mol Cancer* 20(1). England:BioMed Central,2021. 131.
30. Natarajan SR, Krishnamoorthy R, Alshuniaber MA et al. Identification of FOXM1 as a novel protein biomarker and therapeutic target for colorectal cancer progression: Evidence from immune infiltration and bioinformatic analyses. *Int J Biol Macromol*. 282(Pt 4). Netherlands:Elsevier,2024. 137201.
31. Jin Y, Chen DL, Wang F et al. The predicting role of Circulating tumor DNA landscape in gastric cancer patients treated with immune checkpoint inhibitors. *Mol Cancer* 19(1). England:BioMed Central,2020. 154.
32. Zhang L, Wang W, Wang R et al. Reshaping the Immune Microenvironment by Oncolytic Herpes Simplex Virus in Murine Pancreatic Ductal Adenocarcinoma. *Mol Ther*. 29(2). United States:Cell Press,2021. 744–761.
33. Chen L, Hua J, He X. Bioinformatics analysis identifies a key gene HLA_DPA1 in severe influenza-associated immune infiltration. *BMC Genomics* 25(1). England:BioMed Central,2024. 257.
34. Ma T, Tang Y, Wang T et al. Chronic pulmonary bacterial infection facilitates breast cancer lung metastasis by recruiting tumor-promoting MHCII(hi) neutrophils. *Signal Transduct Target Ther*. 8(1). England:Springer Nature,2023. 296.
35. Adrover JM, McDowell S, He XY et al. Networking with cancer: The bidirectional interplay between cancer and neutrophil extracellular traps. *Cancer Cell*. 41(3). United States:Cell Press,2023. 505–526.
36. Singel KL, Segal BH. Neutrophils in the tumor microenvironment: trying to heal the wound that cannot heal. *Immunol Rev*. 273(1). England:Wiley-Blackwell Publishing Ltd,2016. 329–43.
37. Wang SS, Liu W, Ly D et al. Tumor-infiltrating B cells: their role and application in anti-tumor immunity in lung cancer. *Cell Mol Immunol*. 16(1). China:Springer Nature,2019. 6–18.
38. Ding S, Qiao N, Zhu Q et al. Single-cell atlas reveals a distinct immune profile fostered by T cell-B cell crosstalk in triple negative breast cancer. *Cancer Commun (Lond)*. 43(6). United States:other,2023. 661–84.
39. Chu J, Tang S, Li T et al. The role of CD8A in the immune microenvironment of breast cancer. *Front Biosci (Landmark Ed)*. 29(2). Singapore:Bioscience Research Institute,2024. 73.
40. Unterleuthner D, Neuhold P, Schwarz K et al. Cancer-associated fibroblast-derived WNT2 increases tumor angiogenesis in colon cancer. *Angiogenesis*. 23(2). Germany:Springer Netherlands,2020. 159–177.
41. Yang X, Zhang Y, Yang Y et al. Vascular endothelial growth factor-dependent spatiotemporal dual roles of placental growth factor in modulation of angiogenesis and tumor growth. *Proc Natl Acad Sci U S A*. 110(34). United States:other,2013. 13932-7.
42. Bais C, Wu X, Yao J et al. PIGF Blockade does not inhibit angiogenesis during primary tumor growth. *Cell* 141(1). United States:Cell Press,2010. 166–77.
43. Kim SH, Roszik J, Cho SN et al. The COX2 Effector Microsomal PGE2 Synthase 1 is a Regulator of Immunosuppression in Cutaneous Melanoma. *Clin Cancer Res*. 25(5). United States:American Association for Cancer Research Inc,2019. 1650–1663.
44. Bar J, Leibowitz R, Reinmuth N et al. Biological insights from plasma proteomics of non-small cell lung cancer patients treated with immunotherapy. *Front Immunol*. 15Switzerland:Frontiers Media S.A,2024. 1364473.
45. Herrera M, Mezheyeuski A, Villabona L et al. Prognostic interactions between FAP+ Fibroblasts and CD8a+ T cells in colon cancer. *cancer. (Basel)*. 12(11). Switzerland:MDPI (Basel, Switzerland),2020. 3238.
46. Taylor AP, Leon E, Goldenberg DM. Placental growth factor (PGF) enhances breast cancer cell motility by mobilising ERK1/2 phosphorylation and cytoskeletal rearrangement. *Br J Cancer*. 103(1). England:Springer Nature,2010. 82–9.
47. Vandewynckel YP, Laukens D, Devisscher L et al. Placental growth factor Inhibition modulates the interplay between hypoxia and unfolded protein response in hepatocellular carcinoma. *BMC Cancer*. 16England:BioMed Central,2016. 9.

Publisher's note

Springer Nature remains neutral with regard to jurisdictional claims in published maps and institutional affiliations.